

The effect of viscosity on the spherical stability of oscillating gas bubbles

Y. Hao and A. Prosperetti

Department of Mechanical Engineering, The Johns Hopkins University, Baltimore, Maryland 21218

(Received 5 November 1998; accepted 5 March 1999)

Gas bubbles driven in radial oscillations are subject to an instability of the spherical shape that is opposed by surface tension and viscosity. An exact linear formulation for the study of the phenomenon has been available for many years, but its complexity has discouraged a detailed investigation. With the recent theory of sonoluminescence of Lohse and co-workers [Hilgenfeldt *et al.*, *Phys. Fluids*, **8**, 2808 (1996)], there has been a renewed interest in the problem and new data have become available. This paper presents a numerical method for the solution of the pertinent equations and compares the theory with these new data. The coupling of the strong nonlinearity of the bubble radial oscillations with the parametric mechanism of the surface instability results in a very complex structure for the stability boundary. Nevertheless, a good agreement between theory and data is found. A comparison with earlier approximate models is also made. © 1999 American Institute of Physics. [S1070-6631(99)04106-9]

I. INTRODUCTION

The fact that the spherical shape of oscillating gas bubbles may be unstable has long been known experimentally¹⁻³ as well as theoretically.⁴⁻⁷ Recently, renewed interest in this phenomenon has been prompted by the discovery of the intriguing phenomenon of single-bubble sonoluminescence,⁸⁻¹⁰ as it has been hypothesized that the extinction threshold for light emission is due to a shape instability that destroys the bubble.¹¹⁻¹³ For this reason Holt and Gaitan^{14,15} have conducted a new experimental study of the instability threshold of air bubbles in water. The purpose of the present study is to subject the available theory for bubble dynamics and linear shape instability to the stringent test that these new data make available. At the same time, we shall see what is the effect of introducing in the theory several simplifications that have been adopted in the recent sonoluminescence literature. The pressure amplitudes on which we primarily focus here are those for which Holt and Gaitan were able to determine with precision the nature of the surface instability, and are thus lower than those arising in sonoluminescence. Nevertheless, in view of the current interest in this topic, we include some results at higher pressure amplitudes at the end of Sec. V. Further results in this parameter range can be found in a recent paper.¹⁶ The difference between this study and a recent one on the same topic¹⁷ lies in a more realistic treatment of the bubble interior and in the comparison with experiment.

In the last several years there have been a number of studies, referenced and summarized in Ref. 3, on the nonlinear interaction between shape and radial modes for pulsating bubbles. Since we focus here on the linear growth phase of the shape instability, such phenomena are not directly relevant to the subject of this paper.

II. THE STABILITY EQUATION

A theoretical formulation of the spherical stability of a bubble including viscous effects was presented in Ref. 18. The result is based on a linear analysis according to which the bubble shape is perturbed to

$$r = \bar{R}(t) + a_n(t)Y_n^m(\theta, \phi), \quad (1)$$

where R is the instantaneous bubble mean radius, Y_n^m a surface harmonic, and a_n the amplitude of the surface distortion. Since, in the linear regime, the dynamics of the perturbation is independent of the index m , we drop it in the following. It is found that a_n satisfies the following equation:

$$\begin{aligned} \ddot{a}_n + \left[3 \frac{\dot{R}}{R} + 2(n+2)(2n+1) \frac{\nu}{R^2} \right] \dot{a}_n \\ + (n-1) \left[-\frac{\ddot{R}}{R} + (n+1)(n+2) \frac{\sigma}{\rho R^3} + 2(n+2) \frac{\nu \dot{R}}{R^3} \right] a_n \\ + n(n+1) \frac{\dot{R}}{R^2} \int_{R(t)}^{\infty} \left(\frac{R^3}{s^3} - 1 \right) \frac{R^n}{s^n} U(s, t) ds \\ - 2n(n+1)(n+2) \frac{\nu}{R^3} \int_{R(t)}^{\infty} \frac{R^n}{s^n} U(s, t) ds = 0. \end{aligned} \quad (2)$$

Here dots denote time derivatives and ν , ρ , and σ are the kinematic viscosity, density, and surface tension coefficient of the liquid. The field $U(r, t)$, the toroidal component of the liquid vorticity, satisfies

$$\frac{\partial U}{\partial t} + \frac{\partial}{\partial r} \left(\frac{R^2}{r^2} \dot{R} U \right) = \nu \frac{\partial^2 U}{\partial r^2} - n(n+1) \frac{\nu}{r^2} U, \quad (3)$$

subject, at $r = R(t)$, to the boundary condition

$$\begin{aligned}
U(R(t),t) + 2R^{n-1} \int_{R(t)}^{\infty} s^{-n} U(s,t) ds \\
= \frac{2}{n+1} \left[(n+2) \dot{a}_n - (n-1) \frac{\dot{R}}{R} a_n \right]. \quad (4)
\end{aligned}$$

The physical reason for this rather complicated mathematical structure of the problem is that both the amount of vorticity generated at the bubble surface and the viscous damping of the shape oscillations depend on the instantaneous distribution of vorticity. The spatial integrals of the field U are necessary to properly account for this instantaneous distribution.

For small viscosity, since vorticity will be essentially confined to a thin boundary layer proportional to $\sqrt{\nu t}$, one may expect that the integral terms in (2) will be smaller than the other viscous terms. Upon dropping the integrals, one then finds

$$\begin{aligned}
\ddot{a}_n + \left[3 \frac{\dot{R}}{R} + 2(n+2)(2n+1) \frac{\nu}{R^2} \right] \dot{a}_n + (n-1) \\
\times \left[-\frac{\ddot{R}}{R} + (n+1)(n+2) \frac{\sigma}{\rho R^3} + 2(n+2) \frac{\nu \dot{R}}{R^3} \right] a_n = 0. \quad (5)
\end{aligned}$$

In the case of a bubble of fixed radius, one can read from this equation directly the natural frequency of oscillation ω_n and damping constant β_n of the n th mode,

$$\begin{aligned}
\omega_n^2 = (n-1)(n+1)(n+2) \frac{\sigma}{\rho R^3}, \\
\beta_n = (n+2)(2n+1) \frac{\nu}{R^2}. \quad (6)
\end{aligned}$$

These results agree with the classic ones in the literature (see, e.g., Ref. 19).

If one were to wish to go one step beyond this approximation, one would naturally turn to a boundary-layer type approximation. The result would then be^{12,20}

$$\begin{aligned}
\ddot{a}_n + \left[3 \frac{\dot{R}}{R} - 2(n-1)(n+1)(n+2) \frac{\nu}{R^2} \right. \\
+ 2 \frac{n(n+2)^2}{1+2\delta/R} \frac{\mu}{\rho_L R^2} \left. \right] \dot{a}_n \\
+ (n-1) \left[-\frac{\ddot{R}}{R} + (n+1)(n+2) \frac{\sigma}{\rho_L R^3} \right. \\
+ 2 \frac{\nu \dot{R}}{R^3} \left. \left((n+1)(n+2) - \frac{n(n+2)}{1+2\delta/R} \right) \right] a_n = 0, \quad (7)
\end{aligned}$$

where δ is the boundary layer thickness. Brenner *et al.*¹¹ suggest to define this quantity as

$$\delta = \min \left(\sqrt{\frac{\nu}{\omega}}, \frac{R}{2n} \right), \quad (8)$$

in which ω is the frequency of the sound driving the radial oscillations. The quantity $R/2n$ acts as a cutoff justified on the basis of a quasistatic argument¹² for small bubbles.

In Sec. V we shall study how these various approximations compare with the exact result obtained from Eqs. (2), (3), and (4).

III. THE RADIAL MOTION

The model we use for the radial oscillations of the bubble has been documented extensively in our earlier papers and only the pertinent equations will be summarized here.

For the radial equation we use the form of Keller and co-workers,²¹⁻²³

$$\begin{aligned}
\left(1 - \frac{\dot{R}}{c_L} \right) R \ddot{R} + \frac{3}{2} \left(1 - \frac{1}{3} \frac{\dot{R}}{c_L} \right) \dot{R}^2 \\
= \frac{1}{\rho_L} \left(1 + \frac{\dot{R}}{c_L} + \frac{R}{c_L} \frac{d}{dt} \right) [p_B - P_\infty - P_S(t)]. \quad (9)
\end{aligned}$$

In this equation c_L is the speed of sound in the liquid, P_∞ is the static ambient pressure, $P_S(t)$ is the imposed acoustic field pressure evaluated at the location of the bubble, and p_B is the pressure on the liquid side of the interface. This quantity is related to the bubble internal pressure p by the balance of normal stresses across the interface, namely,

$$p = p_B + \frac{2\sigma}{R} + 4\mu \frac{\dot{R}}{R}, \quad (10)$$

in which μ is the liquid viscosity. In this study we take the sound field to be sinusoidal,

$$P_S(t) = P_A \sin \omega t, \quad (11)$$

with P_A the acoustic amplitude and $\omega/2\pi$ the frequency of the driving sound field. Equation (9) is only accurate to first order in the bubble wall Mach number but, for most of the pressure amplitudes of this study, this level of accuracy is sufficient.

A key aspect of the modeling of the radial oscillation is the specification of the internal pressure in the bubble. Here we use a model, described in detail elsewhere (see, e.g., Refs. 24, 25, 26), that accounts for heat transport by convection and conduction inside the bubble. The model has been derived on the assumptions of perfect gas behavior and spatial uniformity of the gas pressure that are well justified for the pressure amplitudes below about 1 bar which are our primary concern. The possible formation of shock waves at higher amplitudes and their role in sonoluminescence and stability are currently a matter of debate.^{10,27-29} It may be mentioned, however, that in an early paper Trilling³⁰ concluded that shocks would not affect significantly the pressure variation at the bubble wall, which is the primary determinant of the radial motion.

The internal pressure p is found by integrating

$$\dot{p} = \frac{3}{R} \left[(\gamma-1)k \frac{\partial T}{\partial r} \Big|_R - \gamma p \dot{R} \right], \quad (12)$$

where γ is the ratio of the specific heats of the gas and k is the gas thermal conductivity. The gas temperature field $T(r,t)$ is obtained from

$$\frac{\gamma}{\gamma-1} \frac{p}{T} \left(\frac{\partial T}{\partial t} + v \frac{\partial T}{\partial r} \right) = \dot{p} + \frac{1}{r^2} \frac{\partial}{\partial r} \left(k r^2 \frac{\partial T}{\partial r} \right), \quad (13)$$

with

$$v = \frac{1}{\gamma p} \left[(\gamma-1) k \frac{\partial T}{\partial r} - \frac{1}{3} r \dot{p} \right]. \quad (14)$$

As shown in Ref. 31, at moderate pressure amplitudes the temperature variations of the liquid at the bubble wall are negligible. Accordingly, we solve (13) assuming, at $r = R(t)$, $T = T_\infty$, where T_∞ is the undisturbed liquid temperature. The gas thermal conductivity is approximated by the linear relation $k = AT + B$, where $A = 5.528 \times 10^{-5}$ W/mK², $B = 0.01165$ W/mK, which closely fits air data over the range $200 \text{ K} < T < 3000 \text{ K}$. For the argon simulations we use instead $A = 3.2 \times 10^{-5}$ W/mK², $B = 0.009$ W/mK.

In view of the complexity of the thermofluid mechanic processes in the bubble, many researchers have used simplified formulations. For example, Lohse and co-workers^{11,12,32,33} calculate the internal pressure from

$$p = \left(P_\infty + \frac{2\sigma}{R_0} \right) \left(\frac{R_0^3 - h^3}{R^3(t) - h^3} \right)^\kappa, \quad (15)$$

where R_0 is the equilibrium radius of the bubble, the polytropic index κ is taken to be 1, and $h = R_0/8.86$ is the hard-core van der Waals radius. In the parameter range of primary concern here it is found that the effect of the parameter h is, however, very small.¹⁶

IV. NUMERICAL ASPECTS

The numerical solution of the problem for a_n is not entirely straightforward and it is appropriate to describe it in some detail.

The first step is to map the interval $R(t) \leq r < \infty$ onto the fixed interval $1 \geq x \geq 0$, which we do by means of the new variable

$$x = \frac{R(t)}{r}. \quad (16)$$

We have also used other mappings with indistinguishable results. Then we expand the field U into a (truncated) series of Chebyshev polynomials of even order,

$$U(r, t) = \sum_0^N u_k(t) T_{2k}(x), \quad (17)$$

which satisfies automatically the condition $\partial U / \partial r \rightarrow 0$ as $r \rightarrow \infty$. The expansion is substituted into the differential equation (3) and the result evaluated at the N collocation points

$$x_k = \cos \frac{\pi k}{2N}, \quad k = 1, 2, \dots, N. \quad (18)$$

The first point x_1 is the node adjacent to the bubble surface and the last one is the point at infinity. In this way, one obtains N equations for the $N+1$ coefficients u_k . The last equation is found from the boundary condition (4). The form of this condition is actually inconvenient for numerical purposes as it establishes an algebraic relation between the u_k 's.

It is more convenient to take a time derivative to find a relation among the derivatives \dot{u}_k . To this end we differentiate (4) with respect to time and use (3) to eliminate the term $\partial U / \partial t$ that arises from the integral, and (4) to eliminate the term $\int_{R^s}^{\infty} r^{-n} U ds$. The final result is

$$\begin{aligned} & \left[\frac{\partial U}{\partial t} + \dot{R} \frac{\partial U}{\partial r} \right]_{R(t)} \\ &= \frac{2(n+2)}{n+1} \ddot{a}_n - \frac{2(n-1)}{n+1} \frac{\dot{R}}{R} \dot{a}_n \\ & \quad - \frac{2(n-1)(n+3)}{n+1} \frac{\dot{R}}{R} \dot{a}_n + \frac{2n(n-1)}{n+1} \frac{\dot{R}^2}{R^2} \dot{a}_n \\ & \quad + \left[(n-1) \frac{\dot{R}}{R} U + 2n \frac{vU}{R^2} + 2 \frac{v}{R} \frac{\partial U}{\partial r} \right]_{r=R} \\ & \quad + 2n \frac{\dot{R}}{R^2} \int_R^\infty \left(\frac{R}{s} \right)^{n+3} U ds. \end{aligned} \quad (19)$$

To generate the numerical results that follow we typically take $N = 16$, which has been determined on the basis of convergence studies to give a good accuracy.

The integrals over the variable r appearing in (2) and (19) are evaluated by Gaussian quadrature after carrying out the change of variable (16). For instance,

$$\int_{R(t)}^\infty \left(\frac{R}{s} \right)^n U ds = \frac{1}{2} R \int_{-1}^1 [x^{n-2} \sqrt{1-x^2} U] \frac{dx}{\sqrt{1-x^2}}. \quad (20)$$

The integral in the right-hand side is in the standard form for Gaussian evaluation using the zeros of Chebyshev polynomials. Typically we use the zeros of T_{16} . Preliminary calculations with a greater number of points, up to the zeros of T_{40} , did not change the results appreciably. We have verified that our results coincide with the recent ones of Ref. 17 when, as in that work, the bubble internal pressure is calculated from (15) with $\kappa = 7/5$ and the prefactor is changed from $P_\infty + 2\sigma/R_0$ to P_∞ .

For the numerical solution of the radial oscillation model, the gas energy equation is transformed into a set of ordinary differential equations by the Chebyshev spectral collocation method described in Refs. 24 and 34. Up to a forcing pressure of 1 bar, we have used 16 and 20 terms in the Chebyshev expansion finding virtually identical results. Above 1 bar, we gradually increased the number of terms up to 40 for 1.45 bars.

V. RESULTS

Hilgenfeldt *et al.*¹² distinguish between 3 types of surface instabilities for oscillating bubbles; parametric, Rayleigh–Taylor, and ‘‘afterbounce.’’ The first one accumulates over time and is similar to the mechanism giving rise to the well-known Faraday waves. The second one is directly linked to the term \ddot{R} in Eq. (2), and manifests itself in a sudden growth of the surface mode when the radial acceleration is strongly positive. The last type of instability grows

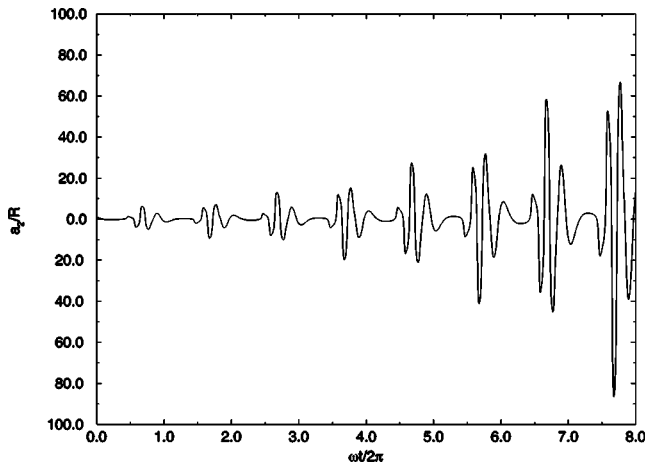


FIG. 1. An example of the development of the $n=2$ shape instability of an air bubble in water for $\omega/2\pi=20.6$ kHz, $P_A=0.8$, $R_0=17$ μm .

parametrically during the rapid afterbounces that bubbles driven far below their natural frequency sometimes execute after the point of minimum radius. While the latter two types of instability are encountered at pressure amplitudes in excess of 1.3 atm with the simplified polytropic model (15) for the bubble internal pressure used, e.g., in Ref. 12, we have shown in a recent paper¹⁶ that they are strongly suppressed by the proper account of thermal effects in the gas that is incorporated in the model of Eqs. (12)–(14). Hence, the only instability that needs to be considered here is of the parametric type. If the instability threshold is evaluated from the boundary-layer approximation (7), one can use Floquet's theorem to calculate the amplification rate after just one period of the (steady-state) radial oscillation. No such theorem is however available for the complete integro-differential model (2) and we have to have recourse to integration over several cycles to judge whether each particular case is stable or unstable. Fortunately, the instability is often violent and the judgment as to its presence is easily made on the basis of its behavior over 5–10 cycles. Typical examples of the development or damping of the instability for an air bubble are shown in Figs. 1 and 2 both for $\omega/2\pi=20.6$ kHz, $n=2$, $P_A=0.8$, with $R_0=17$ and 7 μm , respectively. In other cases, however, the integration was continued for 20–40 cycles to identify a clear trend, and over 100 would have been necessary to see the actual blow-up of the modal amplitude. This circumstance renders the identification of stability boundaries very time consuming, and for this reason some of the results shown below do not display these boundaries in all of their complexity.

Holt and Gaitan^{14,15} give the stability threshold as a function of the bubble equilibrium radius and sound amplitude for air bubbles in water at 20.6 kHz; for 1 bar static pressure, the resonant radius at this frequency is $R_{res}=153$ μm . At pressure amplitudes below 1 bar they were able to identify the order n of the unstable surface mode, and these are the only data that we consider. These data are shown by the open circles in Figs. 3 ($n=2$), 4 ($n=3$), and 5 ($n=4$). The stability threshold of our model corresponds to the boundary between the black and white areas of the

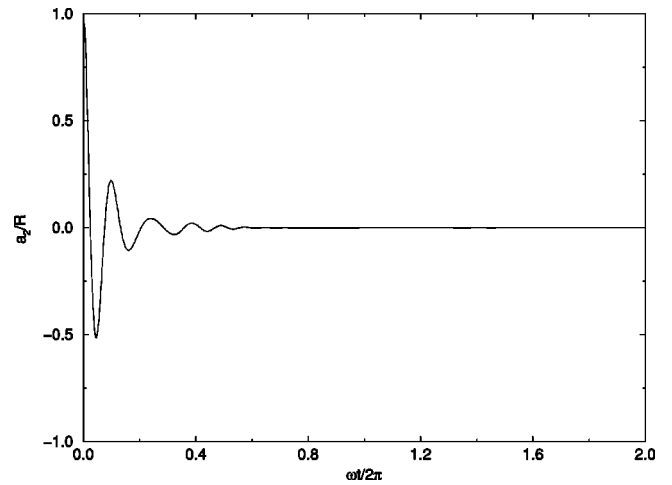


FIG. 2. An example of the damping of the $n=2$ shape instability of an air bubble in water for $\omega/2\pi=20.6$ kHz, $P_A=0.8$, $R_0=7$ μm .

figures. Even though it would be desirable to have data providing a more even coverage of the parameter range, the agreement between theory and experiment is generally good.

The general features of the instability are well understood on the basis of the stability theory for the Mathieu (or, more generally, Hill) equation. As shown in Ref. 35, with the substitution $a_n=b_n/R^{3/2}$, and retaining only terms linear in the radius perturbation, Eq. (2) becomes

$$\frac{d^2 b_n}{d\tau^2} + 2 \frac{\beta_n}{\omega} \frac{db_n}{d\tau} + \left[\frac{\omega_n^2}{\omega^2} + X_0 \theta_n \cos(\tau + \phi) \right] b_n = 0, \quad (21)$$

where $\tau = \omega t$,

$$\theta_n = n + \frac{1}{2} - 3 \frac{\omega_n^2}{\omega_2^2}, \quad (22)$$

and we have set

$$R = R_0 [1 + X_0 \cos(\tau + \phi)]. \quad (23)$$

From a linearization of the model of Sec. III, we have^{25,26}

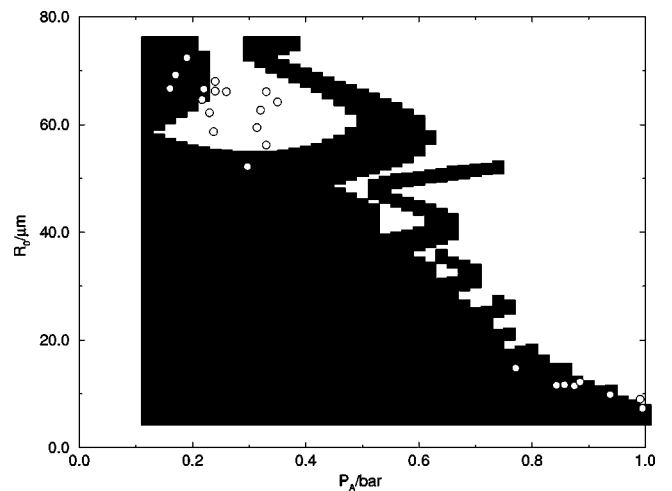


FIG. 3. The dark area is the calculated stability region for the $n=2$ shape mode for an air bubble in water at $\omega/2\pi=20.6$ kHz. The open circles are the data of Holt and Gaitan (1996, 1998).

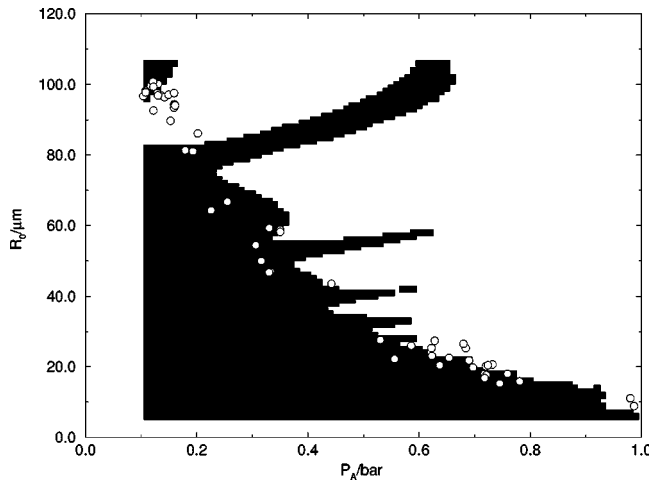


FIG. 4. The dark area is the calculated stability region for the $n=3$ shape mode for an air bubble in water at $\omega/2\pi=20.6$ kHz. The open circles are the data of Holt and Gaitan (1996, 1998).

$$X_0 = \frac{1}{[(\omega^2 - \omega_0^2)^2 + 4\beta^2\omega^2]^{1/2}} \frac{P_A}{\rho R_0^2}, \quad (24)$$

$$\sin \phi = \frac{2\beta\omega}{[(\omega^2 - \omega_0^2)^2 + 4\beta^2\omega^2]^{1/2}},$$

where β is the total damping affecting the radial oscillations and ω_0 the linear resonance frequency of the bubble. The explicit expressions for these quantities are rather complicated and are given in the references. If R in the definitions of β_n and ω_n is kept constant at its equilibrium value R_0 for simplicity, Eq. (21) is in the standard form of the damped Mathieu equation. The stability boundary in the neighborhood of $\omega_n^2/\omega^2 = 1/4$ are given approximately by (see, e.g., Refs. 36 and 37)

$$\left(\frac{\omega_n^2}{\omega^2} - \frac{1}{4}\right)^2 = \frac{1}{4} X_0^2 \theta_n^2 - \frac{\beta_n^2}{\omega^2}. \quad (25)$$

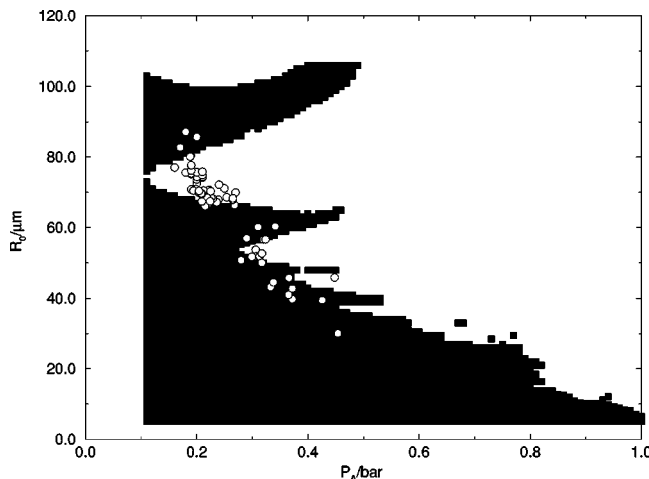


FIG. 5. The dark area is the calculated stability region for the $n=4$ shape mode for an air bubble in water at $\omega/2\pi=20.6$ kHz. The open circles are the data of Holt and Gaitan (1996, 1998).

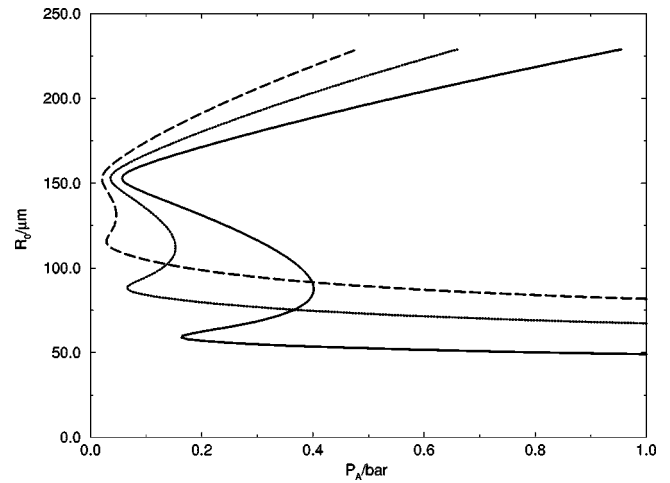


FIG. 6. Stability boundary (25) for the Mathieu equation (21) expressed in terms of the pressure amplitude and bubble radius for the $n=2$ (solid line), 3 (dotted line), and 4 (dashed line). The radial oscillations are described by the linearized theory.

A graph of this boundary expressed as R_0 vs P_A for an air bubble in water is shown in Fig. 6 for $n=2$ (solid line), 3 (dotted line), and 4. The double dips in these curves can be explained by observing that (25) would give an instability near $\omega_n^2/\omega^2 = 1/4$ even with a constant (sufficiently large) X_0 . As the resonance frequency of the bubble oscillation is approached, however, X_0 increases, with the effect that the instability extends to a greater distance from $1/4$. This accounts for the second minimum around $R_0 = 153 \mu\text{m}$. The minimum in the instability threshold around $R_0 = 60 \mu\text{m}$ indicated in Fig. 6 for $n=2$ is reflected in a minimum in the full stability map of Fig. 3, and similarly the minimum for $n=3$ around $R_0 = 87 \mu\text{m}$ can be seen in Fig. 4, and the minimum around $R_0 = 115 \mu\text{m}$ for $n=4$ is present in Fig. 5. The Mathieu equation has instability regions also for $\omega_n^2/\omega^2 = M^2$ with $M=1,2,\dots$, and it can therefore be expected that the double dip structure of Fig. 6 would be associated to many more of these unstable modes, although the effect of damping becomes progressively stronger as the order M is increased.

The previous simple argument relies on the presence of a single resonance for the bubble oscillations. Actually, as shown in Fig. 7, these oscillations are strongly nonlinear and one therefore expects a Mathieu-equation structure similar to the one just described associated to all the nonlinear radial resonances. This fact might explain the S-shaped stable regions in the $n=2$ stability map. For example, near $R_0 \approx 50 \mu\text{m}$, there is a resonance at the third harmonic which gives rise to the stability threshold near $P_A \approx 0.46$ bars. According to the Mathieu diagram in Fig. 6, one expects stability of this component in a region above a curve starting at $R_0 = 50 \mu\text{m}$ and $P_A \approx 0.46$ bars. The stability region that one encounters in Fig. 3 around $R_0 \approx 60 \mu\text{m}$ and $P_A \approx 0.5-0.6$ bars may be a consequence of the competition between the destabilizing effect of the fundamental mentioned before, and the stabilizing effect of this third harmonic. Whatever the explanation of these particular features, one would expect that the combination of the complex stability

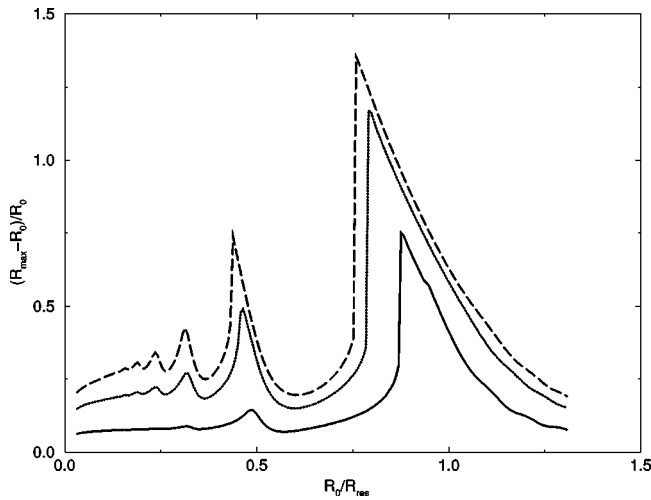


FIG. 7. Dimensionless maximum radius of the bubble in the course of steady oscillations as a function of equilibrium radius for pressure amplitudes of 0.2 (solid line), 0.4 (dotted line), and 0.5 (dashed line) bars for an air bubble in water at $\omega/2\pi = 20.6$ kHz as predicted by the model of Sec. III.

boundary of the Mathieu (or Hill) equation and the nonlinear features of the radial oscillations can account for the intricacy of the stability boundaries.

Qualitatively, the complexity of these boundaries seems to decrease as n increases. This feature can be understood by noting that the resonances $\omega_n^2/\omega^2 = M^2$ of the Mathieu equation occur for

$$R_0 = \left[\frac{(n-1)(n+1)(n+2)}{M^2} \frac{\sigma}{\rho\omega^2} \right]^{1/3} \quad (26)$$

Thus, as n increases, the region $R_0 \leq 80 \mu\text{m}$ corresponds to higher and higher M , and is therefore more sensitive to the action of viscosity on the instability.

Figure 8 shows the stability boundary for $n=2$ as computed with the boundary layer approximation together with the complete model of Sec. III for the radial oscillations.

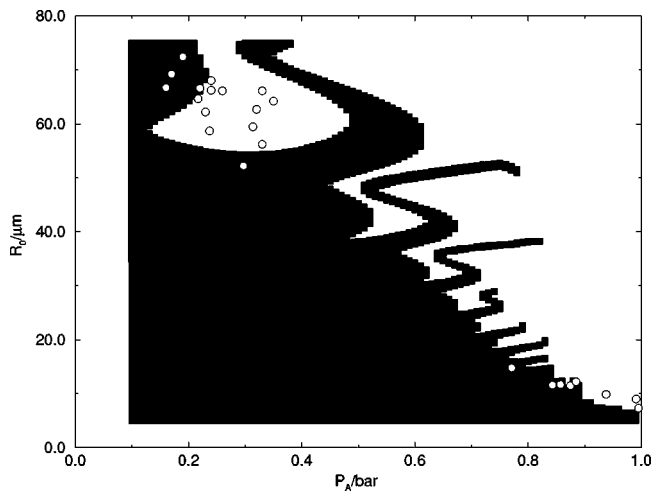


FIG. 8. Stability region for the $n=2$ shape mode as computed with the boundary layer approximation (7) together with the complete model of Sec. III for the radial oscillations. At the higher pressures Fig. 3 indicates that the complete model is slightly more stable than the boundary layer one. The stability regions below about 0.5 bars are practically coincident.

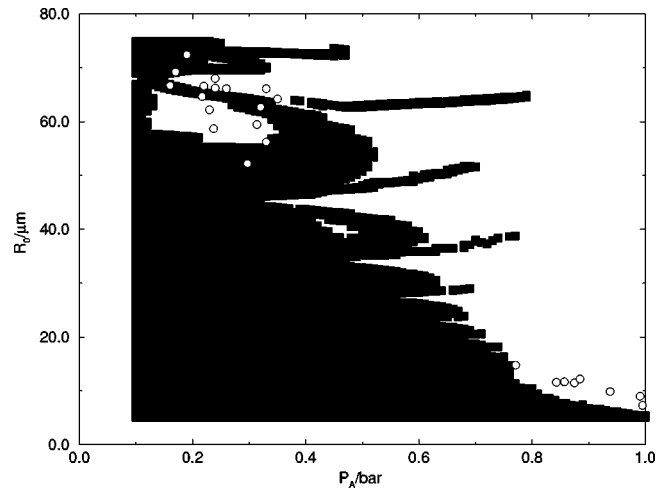


FIG. 9. Stability region for the $n=2$ shape mode as computed with the boundary layer approximation (7) for isothermal bubble oscillations. The shape of the stability boundary for the larger radii is significantly different from the exact results of Fig. 3. At higher pressures, the complete model is significantly more stable.

Upon comparison with Fig. 3, we notice a substantial agreement at the lower pressure amplitudes $P_A < 0.6-0.7$ bars. At higher amplitudes, however, the complete model is more stable than the boundary layer one, and is seen to agree better with the data in the region $0.9 < P_A < 1$ bars. The corresponding result for the boundary layer approximation coupled with isothermal bubble oscillations are shown in Fig. 9, where the difference with the data are appreciably greater.

Before we have remarked on the difficulty of determining with precision the stability boundary from the theory of Sec. II. In order to give a better sense of the accuracy of the results given in the previous figures, for $n=2$ we have investigated in greater (if still somewhat insufficient) detail a small region of the relevant parameter space. The results are shown in Fig. 10 where the thin solid line is the stability threshold plotted in Fig. 3, the thick solid line the same threshold computed with a finer resolution, the dotted line is the boundary layer result, and the dashed line (under all the others) is the boundary layer/isothermal bubble model. It is seen that, with a finer sampling of the (R_0, P_A) plane, more features are uncovered of which the less detailed results of Fig. 3 are a “filtered” version. From the appearance of these curves it is however also apparent that yet finer features are present, as can also be deduced from the lines showing the boundaries calculated from the approximate models. (As pointed out before, it is easier to bring out finer details of these boundaries due to the applicability of Floquet’s theorem.) In view of the difficulty and tediousness of this detailed analysis (and of the fact that the data are not accurate enough to warrant such a fine comparison) we do not pursue it further. In general, however, as noticed in Ref. 17, it can be seen that there is a tendency for the boundary layer model (dotted line) to slightly underestimate the threshold at the lower pressure amplitudes. When the boundary layer model is coupled with the isothermal approximation (lowest dashed line), this tendency is markedly increased.

It is also interesting to compare the stability features of

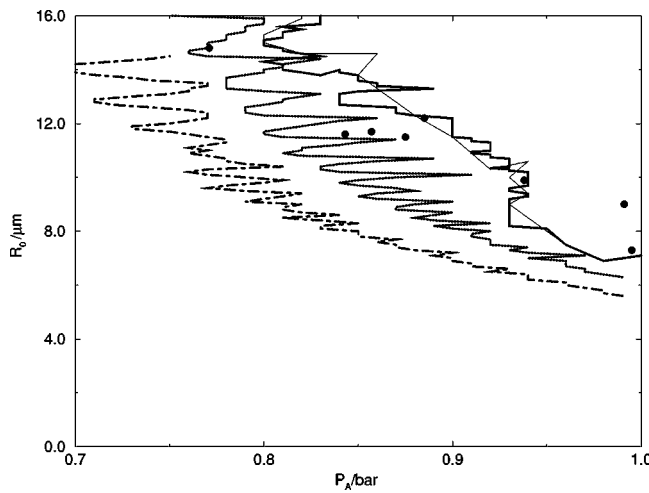


FIG. 10. The thin solid line is part of the stability boundary for $n=2$ plotted in Fig. 3. The thick solid line represents the result of a better approximation to this boundary resulting from a finer discretization of the parameter space. The dotted line is the result of the complete model for the radial dynamics coupled with the boundary-layer approximation (7), (8) for the viscous effects. The dashed line is the boundary layer approximation with an isothermal model for the bubble oscillations.

an argon bubble with those of an air bubble. For simplicity we do this by calculating viscous effects with the boundary layer approximation. Figure 11 shows such results for the $n=2$ mode. The argon bubble (solid line) is found to be somewhat more stable than the air bubble (dashed line). The difference between the radius, radial velocity, and radial acceleration are illustrated in Fig. 12 for $R_0=8.6 \mu\text{m}$ and $P_A=0.91$ bars. In this case the air bubble (dashed lines) is unstable, while the argon bubble (solid lines) is stable. The difference in behavior between the two cases is mostly due to the different values of the adiabatic index γ . It is seen that the air bubble oscillations are stronger, with greater velocity extrema and, more importantly, much larger outward (and, therefore, destabilizing) radial accelerations.

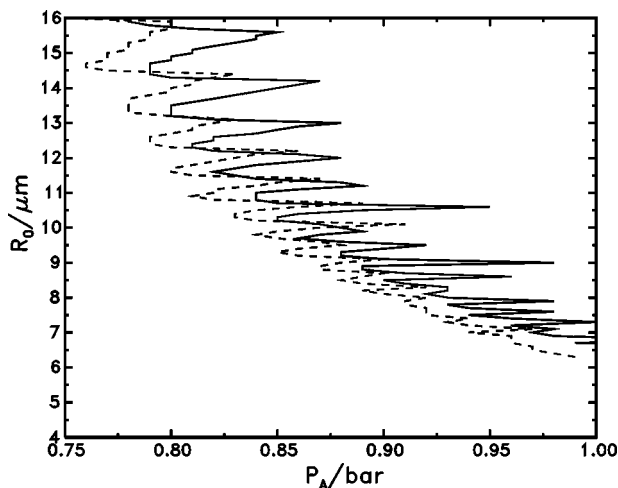


FIG. 11. Comparison between the stability boundaries for the $n=2$ mode of an argon bubble (solid line) and an air bubble (dashed line) computed with the boundary layer approximation to viscous effects and the complete model of Sec. III for the radial motion.

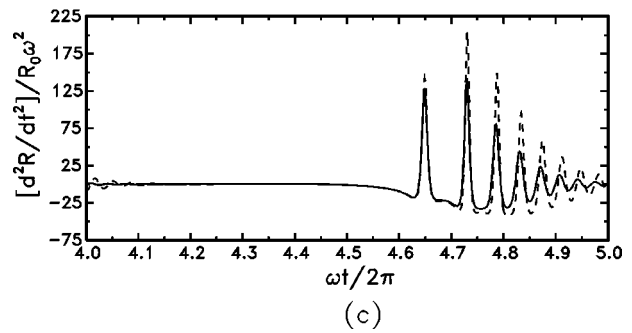
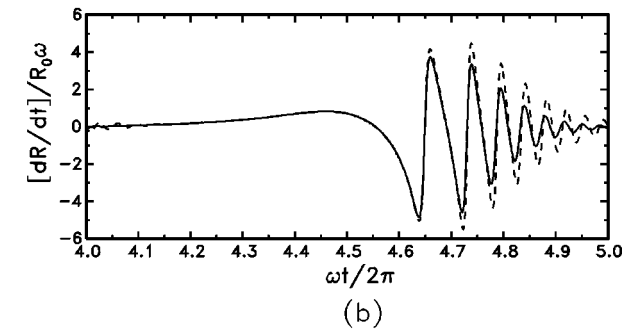
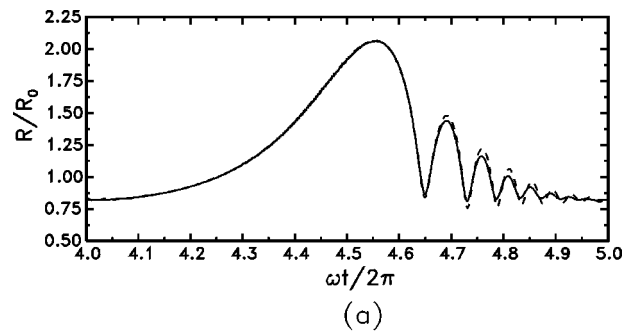


FIG. 12. Comparison between (a) the radius, (b) the radial velocity, and (c) the radial acceleration of an argon bubble (solid lines) and an air bubble (dashed lines). The equilibrium radius is $R_0=8.6 \mu\text{m}$ and the pressure amplitude $P_A=0.91$ bars. For the $n=2$ mode, with these parameter values the air bubble is unstable while the argon bubble is stable.

The range of pressure amplitudes explored thus far is below that where sonoluminescence is encountered. Although the purpose of this paper is to compare the theory with the available data, it may be interesting to conclude with the presentation of the stability boundary for an argon bubble extending into the sonoluminescence region. Due to numerical difficulties (a failure to converge in the time integration), we have been unable to calculate this boundary with the complete viscous model of Sec. II. Thus we content ourselves with relatively low-resolution results obtained with the boundary layer approximation that, as shown in Ref. 17, is affected by a smaller error in this parameter range. The solid line in Fig. 13 is the stability boundary found with the complete radial model of Sec. III, and the dotted line that with the simplified isothermal pressure relation (15). Although, below 1.2 bars, the isothermal model lies below the other one in keeping with the pattern encountered in Fig. 10, above 1.2 bars the two results are very close. A similar comparison between the isothermal and full radial models at a somewhat higher frequency, 26.5 kHz, was presented in Ref.

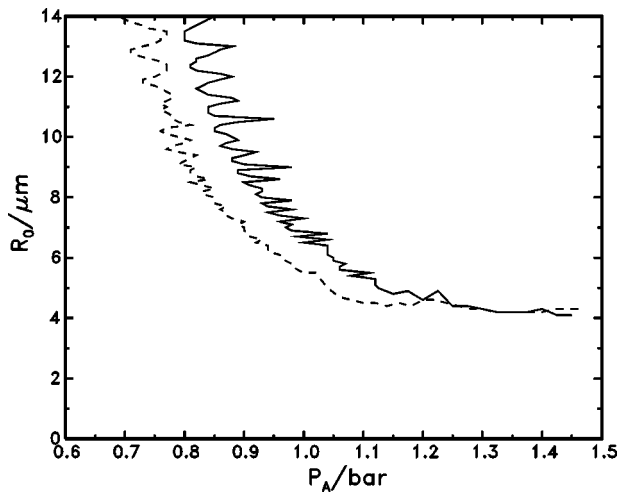


FIG. 13. Comparison between the stability boundaries for the $n=2$ mode of an argon bubble as computed with the complete radial model of Sec. III (solid line) and the isothermal approximation (15) (dashed line). In both cases, viscous effects are treated in the boundary layer approximation.

16 where the isothermal model was found to underpredict the stability threshold in this same pressure range. These results indicate that the mutual relationship between the thresholds predicted by the two models depends upon the precise conditions, and it would be difficult to make general statements, particularly at the higher pressure amplitudes. As pointed out in Ref. 32, air decomposes at these higher sound pressure amplitudes and, for this reason, we do not show similar results for air bubbles.

VI. CONCLUSIONS

In this paper we have compared the available theory for the stability of the spherical shape of a radially oscillating bubble with some recent experimental data by Holt and Gaitan.^{14,15} The theory is phrased in terms of an integrodifferential formulation that renders the evaluation of the stability boundaries rather complicated. A numerical method for this purpose has been developed and shown to lead to results in good agreement with data, particularly for pressure amplitudes above 0.5 bars (Figs. 3 and 4).

At lower amplitudes the agreement is not as good. In addition to the complex structure of the stability boundary in this range, a probable reason is that here bubbles are larger. With increasing radius, surface tension is less and less able to maintain sphericity in the presence of gravity, acoustic streaming, and other perturbations and the stability features of a distorted bubbles are expected to be different from those of a spherical one.^{38,3}

ACKNOWLEDGMENTS

The authors express their gratitude to Dr. R. G. Holt and Dr. F. Gaitan for making their shape stability data available. This study has been supported by NASA.

- ¹N. Gaines, "Magnetostriction oscillator producing intense audible sound and some effects obtained," *Physics (N.Y.)* **3**, 209 (1932).
- ²M. Kornfeld and L. Suvorov, "On the destructive action of cavitation," *J. Appl. Phys.* **15**, 495 (1944).
- ³Z. C. Feng and L. G. Leal, "Nonlinear bubble dynamics," *Annu. Rev. Fluid Mech.* **29**, 201 (1997).
- ⁴M. S. Plesset, "On the stability of fluid flows with spherical symmetry," *J. Appl. Phys.* **25**, 96 (1954).
- ⁵G. Birkhoff, "Note on Taylor instability," *Q. Appl. Math.* **12**, 306 (1954).
- ⁶G. Birkhoff, "Stability of spherical bubbles," *Q. Appl. Math.* **13**, 451 (1956).
- ⁷A. I. Eller and L. A. Crum, "Instability of the motion of a pulsating bubble in a sound field," *J. Acoust. Soc. Am.* **47**, 762 (1970).
- ⁸D. F. Gaitan and L. A. Crum, "Observation of sonoluminescence from a single, stable cavitation bubble in a water/glycerine mixture," in *Frontiers in Nonlinear Acoustics*, edited by M. Hamilton and D. T. Blackstock (Elsevier, New York, 1990), pp. 459–463.
- ⁹D. F. Gaitan, L. A. Crum, C. C. Church, and R. A. Roy, "Sonoluminescence and bubble dynamics from a single, stable, cavitation bubble," *J. Acoust. Soc. Am.* **91**, 3166 (1992).
- ¹⁰B. P. Barber, R. A. Hiller, R. Löfstedt, S. J. Putterman, and K. R. Weninger, "Defining the unknowns of sonoluminescence," *Phys. Rep.* **281**, 65 (1997).
- ¹¹M. P. Brenner, D. Lohse, and T. F. Dupont, "Bubble shape oscillations and the onset of sonoluminescence," *Phys. Rev. Lett.* **75**, 954 (1995).
- ¹²S. Hilgenfeldt, D. Lohse, and M. P. Brenner, "Phase diagrams for sonoluminescing bubbles," *Phys. Fluids* **8**, 2808 (1996); **9**, 2462(E) (1996).
- ¹³S. Grossman, S. Hilgenfeldt, D. Lohse, and M. Zomack, "Sound radiation of 3 MHz driven gas bubbles," *J. Acoust. Soc. Am.* **102**, 1223 (1997).
- ¹⁴R. G. Holt and D. F. Gaitan, "Observation of stability boundaries in the parameter space of single bubble sonoluminescence," *Phys. Rev. Lett.* **77**, 3791 (1996).
- ¹⁵R. G. Holt and D. F. Gaitan, "Experimental observations of bubble response and light intensity near the threshold for single bubble sonoluminescence in an air–water system," to appear in *Phys. Rev.*
- ¹⁶A. Prosperetti and Y. Hao, "Modeling of spherical gas bubble oscillations and sonoluminescence," *Philos. Trans. R. Soc. London* **A357**, 203 (1999).
- ¹⁷C. C. Wu and P. H. Roberts, "Bubble shape instability and sonoluminescence," *Phys. Lett. A* **250**, 131 (1998).
- ¹⁸A. Prosperetti, "Viscous effects on perturbed spherical flows," *Q. Appl. Math.* **34**, 339 (1977).
- ¹⁹H. Lamb, *Hydrodynamics*, 6th ed. (Cambridge University Press, Cambridge, 1932).
- ²⁰A. Prosperetti, "On the stability of spherically symmetric flows," *Atti Accad. Naz. Lincei, Cl. Sci. Fis. Mat. Nat. Rend.* **62**, 196 (1977).
- ²¹J. B. Keller and I. I. Kolodner, "Damping of underwater explosion bubble oscillations," *J. Appl. Phys.* **27**, 1152 (1956).
- ²²J. B. Keller and M. J. Miksis, "Bubble oscillations of large amplitude," *J. Acoust. Soc. Am.* **68**, 628 (1980).
- ²³A. Prosperetti and A. Lezzi, "Bubble dynamics in a compressible liquid. Part I. First-order theory," *J. Fluid Mech.* **185**, 289 (1986).
- ²⁴V. Kamath and A. Prosperetti, "Numerical integration methods in gas-bubble dynamics," *J. Acoust. Soc. Am.* **85**, 1538 (1989).
- ²⁵A. Prosperetti, L. A. Crum, and K. W. Commander, "Nonlinear bubble dynamics," *J. Acoust. Soc. Am.* **83**, 502 (1988).
- ²⁶A. Prosperetti, "The thermal behaviour of oscillating gas bubbles," *J. Fluid Mech.* **222**, 587 (1991).
- ²⁷C. C. Wu and P. H. Roberts, "Shock-wave propagation in a sonoluminescing gas bubble," *Phys. Rev. Lett.* **70**, 3424 (1993).
- ²⁸W. C. Moss, D. B. Clarke, and D. A. Young, "Calculated pulse widths and the spectra of a single sonoluminescing bubble," *Science* **276**, 1398 (1997).
- ²⁹V. Q. Vuong, A. J. Szeri, and D. A. Young, "Shock formation within sonoluminescence bubbles," *Phys. Fluids* **11**, 10 (1999).
- ³⁰L. Trilling, "The collapse and rebound of a gas bubble," *J. Appl. Phys.* **23**, 14 (1952).
- ³¹V. Kamath, A. Prosperetti, and F. Egolfopoulos, "A theoretical study of sonoluminescence," *J. Acoust. Soc. Am.* **94**, 248 (1993).

- ³²D. Lohse and S. Hilgenfeldt, "Inert gas accumulation in sonoluminescing bubbles," *J. Chem. Phys.* **107**, 6986 (1997).
- ³³S. Hilgenfeldt, D. Lohse, and W. C. Moss, "Water temperature dependence of single bubble sonoluminescence," *Phys. Rev. Lett.* **80**, 1332 (1998).
- ³⁴Y. Hao and A. Prosperetti, "The dynamics of vapor bubbles in acoustic pressure fields," *Phys. Fluids* (in press).
- ³⁵A. Prosperetti, "Bubble phenomena in sound fields: Part two," *Ultrasonics* **22**, 115 (1984).
- ³⁶L. D. Landau and E. M. Lifshitz, *Mechanics* (Pergamon, Oxford, 1959).
- ³⁷D. W. Jordan and P. Smith, *Nonlinear Ordinary Differential Equations* (Clarendon, Oxford, 1979).
- ³⁸W. T. Shi and R. E. Apfel, "Deformation and position of acoustically levitated liquid drops," *J. Acoust. Soc. Am.* **99**, 1977 (1996).